International Forum on Aeroelasticity and Structural Dynamics
IFASD 2024
17-21 June 2024, The Hague, The Netherlands

SHAPE IDENTIFICATION OF A WING MODEL BY ADDITIVE MANUFACTURING FOR TRANSONIC WIND TUNNEL TESTING

Natsuki Tsushima[1,2], Holger Mai[3], Marc Braune[3], Thomas Buete[3]

[1] Japan Aerospace Exploration Agency, Chofu, 182-0012 Tokyo, Japan
[2] The University of Tokyo, Hongo, 113-8656 Tokyo, Japan
[3] DLR-Institute of Aeroelasticity, 37073 Göttingen, Germany

Keywords: Additive manufacturing, Transonic wing model, Strain sensors, Structural monitoring

Abstract: Additive manufacturing with a higher degree of design and manufacturing freedom has the potential to enhance structural performance and capability. The technique may also help to effectively perform wind tunnel testing. This paper aims to explore a structural shape identification technique for additively manufactured wing structures to enhance the capability of additively manufactured wing models for transonic wind tunnel testing. The objectives of this paper are 1) to explore the feasibility and capability of a method for the structural shape identification of additively manufactured solid wing structures based on strain measurements, and 2) to design an integrated structural monitoring system into AM-based transonic wing models, which enables the effective construction and investigation of aeroelastic wing models, and 3) to investigate the prediction accuracy for deformations of such a wing model. Ko's displacement theory was applied to identify structural deformations of wing structures based on strain measurements in this study. Based on the numerical results, it was shown that Ko's theory could provide good predictions even for the deformations of a solid swept and tapered wing with an unsymmetric airfoil. The aeroelastic simulation proved that the shape prediction of such a wing model based on the designed strain measurement system and Ko's theory could provide sufficient accuracy for deformation monitoring.

1 INTRODUCTION

Additive manufacturing (AM) technology has been developed at a rapid pace and enabled the realization of conceptual structures that had been difficult to fabricate before. AM technology with a higher degree of design and manufacturing freedom has the potential to enhance structural performance and capability [1, 2]. The technique would also help to effectively perform wind tunnel testing at lower costs. It has been shown that additively manufactured models are capable of providing reliable experimental results for investigations of aerodynamic characteristics in wind tunnel testing for simple experimental conditions in which models are considered "rigid" [3]. Our previous works have also shown the capability of the AM technique to realize not only pure aerodynamic investigations but also evaluations of the aeroelastic characteristics of flexible wing models [4-6].

Critical challenges in aeroelastic wind tunnel testing are related to the precise and dense information of structural and aerodynamic measurements during the experiments. With the help

of the information, a safe and accurate investigation could be performed. To this aim, integrated measurement systems, such as embedded structural health monitoring systems, have been studied in the literature [7-9]. Among the recent enabling technologies, for example, fiber Bragg gratings (FBGs) have shown a promising potential to realize measurement networks for static/dynamic strain measurements and structural shape identification based on strain measurements. Ko's displacement theory [8] especially has the advantage of identifying structural deformations of wing structures based on strain measurements only with a few strain-sensing arrays. By taking advantage of AM technology, effective integrations of fiber optic sensors (FOSs) into structures have been explored. One approach to integrate FOSs into an additively manufactured structure is to embed FOSs in structures during the layer-by-layer stacking process of AM. This approach offers ease of FOS integration by creating sensor channels in the structures and installing FOSs in the channels during the AM process [10-12]. Since the FOSs and channels are simply closed by following layers, no additional post-processing for the installations is required. However, the direction of FOS installation with the approach is limited as the FOSs can be installed only in the building plane on the top layer during the paused layer stacking sequence. Wing models for wind tunnel testing require precise airfoil profiles to realize accurate aerodynamic characteristics. Consequently, it is preferred to align the spanwise direction along the layer stacking direction. Therefore, the practical integration of the strain measurement systems into wing structures remains to be overcome.

In this paper, a structural shape identification technique for additively manufactured wing structures is explored to enhance the capability of additively manufactured wing models for transonic wind tunnel testing. The objectives of this paper are 1) to explore the feasibility and capability of a method for the structural shape identification of additively manufactured solid wing structures based on strain measurements, and 2) to design an integrated structural monitoring system into AM-based transonic wing models, which enables the effective construction and investigation of aeroelastic wing models, and 3) to investigate the prediction accuracy for deformations of such a wing model. Ko's displacement theory is applied to identify structural deformations of wing structures based on strain measurements in this study. Since the theory is mainly studied for simple symmetric beams or wings, the feasibility of the theory to identify structural deformations of unsymmetric solid wings with a supercritical airfoil is first investigated. As a course toward the effective structural monitoring system, the integration of traditional strain gauge measurements is considered. The accuracy of structural shape identification with the strain measurements integrated into additively manufactured structures is then evaluated.

2 THEORETICAL FORMULATION

Ko's displacement theory [8] is used to identify structural deformations of wing structures based on strain measurements. The theory is briefly described in this section.

The vertical deflection of a beam is formulated based on the classical beam equation given by

$$\frac{d^2 z}{dx^2} = \frac{M(x)}{EI} \tag{1}$$

where z is the deflection, x is the spanwise location, $M(x)$ is the bending moment, E is Young's modulus, and I is the moment of inertia of the beam. The bending stress $\sigma(x)$ at the cross-section of the beam is obtained as

$$\sigma(x) = \frac{M(x)c}{I} \tag{2}$$

where c is the distance from the neutral plane of the beam to the strain measurements. The relation between the bending stress and the bending strain $\varepsilon(x)$ gives the bending moment expressed as

$$M(x) = EI\frac{\varepsilon(x)}{c(x)} \tag{3}$$

The beam equation in Eq.(1) is now rewritten as

$$\frac{d^2 z}{dx^2} = \frac{\varepsilon(x)}{c(x)} \tag{4}$$

The advantage of the theory is that the beam equation contains only the distance c and the bending strain without the flexural rigidity EI.

The theory can be extended to obtain deformations of a wing structure by using two arrays of strain measurements as shown in Fig.1. The two strain measurement arrays can be installed along the wing structure away from the neutral plane of the wing. The two arrays can be located between the leading/trailing edge of the wing and the neutral axis with chordwise distance $d(x)/2$. The local deflections z_i^F and z_i^R of the front and rear arrays at the cross-section, x_i, can be estimated by integrating the local strains ε_i and distances c_i. The subscript i indicates the index of strain sensing stations ranging from zero to n. In the discrete form, the local deflections at each strain measurement station are given as

$$\begin{aligned} z_i^F &= \frac{\left(\Delta l^F\right)^2}{6}\sum_{j=1}^{i}\frac{1}{c_{i-j}^F}\left\{\left[3(2j-1)-(3j-2)\frac{c_{i-j+1}^F}{c_{i-j}^F}\right]\varepsilon_{i-j}^F+(3j-2)\varepsilon_{i-j+1}^F\right\}+z_0^F+(i)\Delta l^F\tan\theta_0^F \\ z_i^R &= \frac{\left(\Delta l^R\right)^2}{6}\sum_{j=1}^{i}\frac{1}{c_{i-j}^R}\left\{\left[3(2j-1)-(3j-2)\frac{c_{i-j+1}^R}{c_{i-j}^R}\right]\varepsilon_{i-j}^R+(3j-2)\varepsilon_{i-j+1}^R\right\}+z_0^R+(i)\Delta l^R\tan\theta_0^R \end{aligned} \tag{5}$$

where Δl is the length between the neighboring sensing stations along the arrays, and $\tan\theta_0$ is the slope at the root of the wing. The superscript F and R indicate the variables for the front and rear arrays. The bending deflections can be obtained with an elimination of the torsional components of total deflections by averaging the front and rear deflections. Note that the deflections and slopes at the wing root are zero (i.e., $z_0^F = z_0^R = \tan\theta_0^F = \tan\theta_0^R = 0$) for the cantilevered conditions.

The cross-sectional twist angle ϕ_i at the cross-section x_i can be expressed as

$$\phi_i = \sin^{-1}\left(\frac{z_i^F - z_i^R}{d_i}\right) \tag{6}$$

where ϕ_0 is also zero at the wing root for the cantilevered conditions.

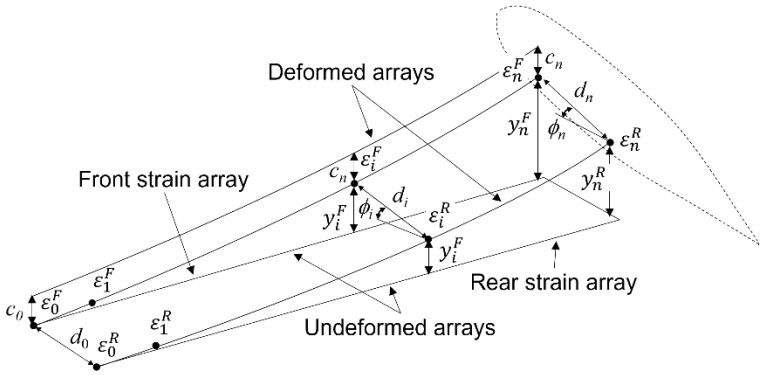

Figure 1: A solid wing with two strain measurement arrays.

3 VERIFICATION OF WING SHAPE IDENTIFICATION

The methodology for the shape identification of unsymmetric solid wings by using strain measurements based on Ko's displacement theory was validated numerically. Four different wing models, as shown in Fig. 2, were considered: (1) unswept straight wing, (2) simply tapered wing (angle between the neutral axis and the y axis is zero), (3) simply swept wing (no taper), and (4) swept and tapered wing. The two strain measurement arrays were installed at the fore and aft of the neutral axis on the wing for each case. A series of finite element simulations were performed by MSC.Nastran to evaluate strains and deformations of each wing. Predictions of deformations based on Ko's displacement theory and the solutions from the finite element simulations were then compared for validation purposes. The geometries of the four wings are summarized in Table 1. The solid wings had the profile of a supercritical airfoil, which was adopted from a wing of JAXA's Technology Reference Aircraft [13]. The neutral axis was located at 39% of the chord. The span and root chord lengths were 500.00 and 202.25 mm. Each wing is subjected to a vertical load of P = 100 N on the neutral axis at the tip of the wing. The wing models were constructed with 60,000 solid HEX8 elements (100 spanwise elements). The distances of c and d at the root of the wings were 10 and 120 mm from the neutral plane and axis for each wing unless otherwise stated. Note that the strain measurement arrays were assumed to be installed within the solid wing structures with the values of c and d. The predicted deformations based on Ko's displacement theory were calculated by using strains on all nodes along each axis/array for the evaluations.

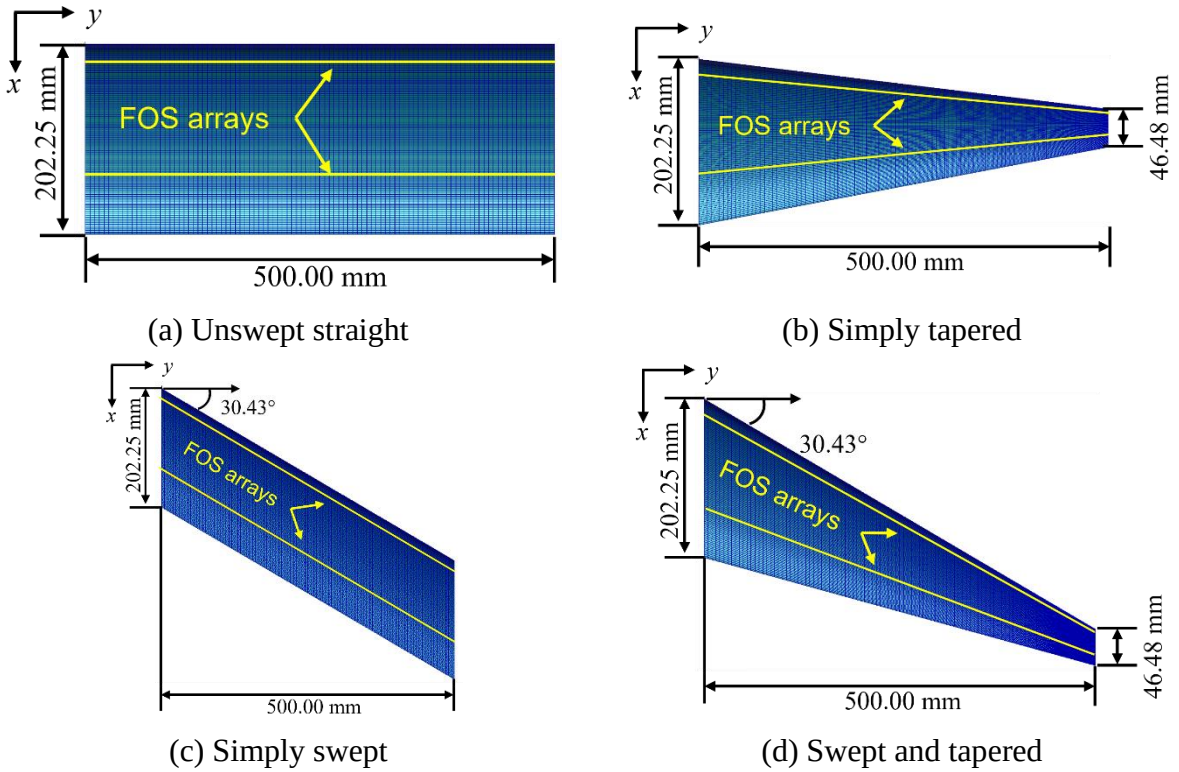

(a) Unswept straight

(b) Simply tapered

(c) Simply swept

(d) Swept and tapered

Figure 2: Four different solid wings with two strain measurement arrays.

Table 1: Geometries of wing models.

Property	Unswept, untapered	Unswept, tapered	Swept, untapered	Swept, tapered
Span, mm	500.00	500.00	500.00	500.00
Root chord, mm	202.25	202.25	202.25	202.25
Taper ratio	1.0	0.23	1.0	0.23
Sweep angle, deg	0.00	--	30.43	27.00

3.1 Unswept straight wing

The unswept straight solid wing studied is shown in Fig. 2a. Figure 3 shows the strains along the front and rear strain measurement arrays on the unswept straight wing, obtained from the finite element simulation. The strain distributions on the two arrays were very similar around the neutral axis. Both strains were almost linear at the outer span. Figure 4 shows the predicted deflections and twist along the strain measurement arrays obtained by Ko's theory. The results showed excellent agreements between the solutions of the finite element simulations and the predictions of Ko's theory based on the strains.

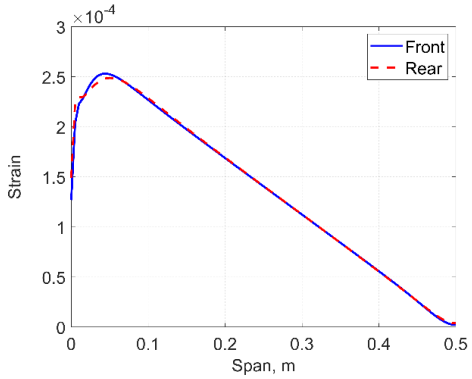

Figure 3: Strains along the front and rear arrays on the unswept straight wing.

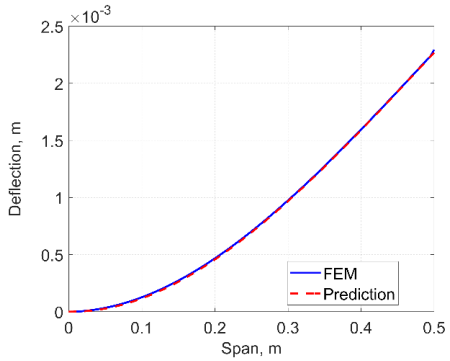

(a) deflection along the neutral axis

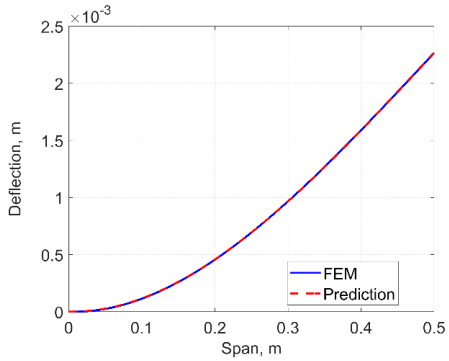

(b) deflection along the front array

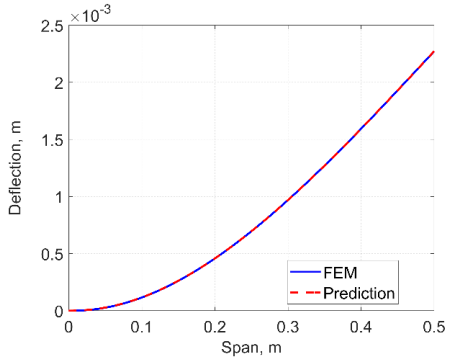

(c) deflection along the rear array

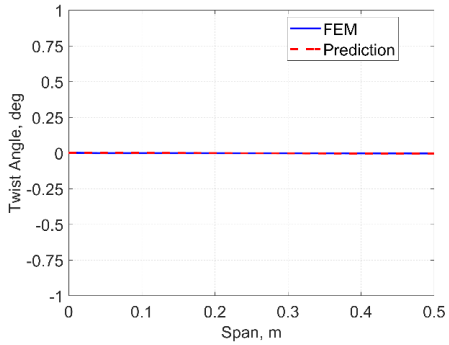

(d) twist along the neutral axis

Figure 4: Comparisons of deflections and twists along the neutral axis and strain measurement arrays on the unswept straight wing predicted by Ko's theory.

3.2 Simply tapered wing

The simply tapered solid wing studied is shown in Fig. 2b. Figure 5 shows the strains along the front and rear strain measurement arrays on the simply tapered wing, obtained from the finite element simulation. The strain distributions on the two arrays were still almost the same. However, the strains increased as the location approached the tip. They dropped then close to zero around the tip region. Figure 6 shows the predicted deflections and twist along the two arrays obtained by Ko's theory. The results also showed excellent agreements between the solutions of the finite element simulations and the predictions of Ko's theory based on the strains.

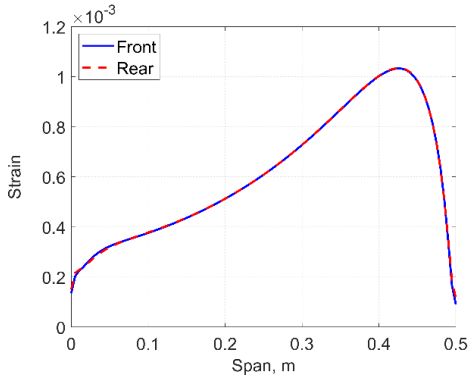

Figure 5: Strains along the front and rear arrays on the simply tapered wing.

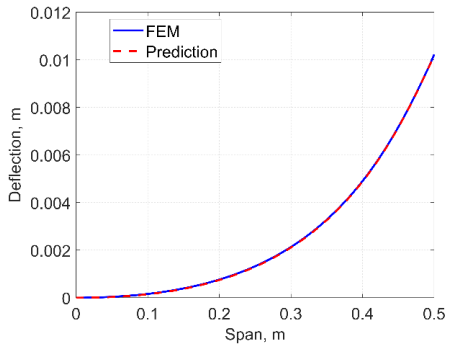

(a) deflection along the neutral axis

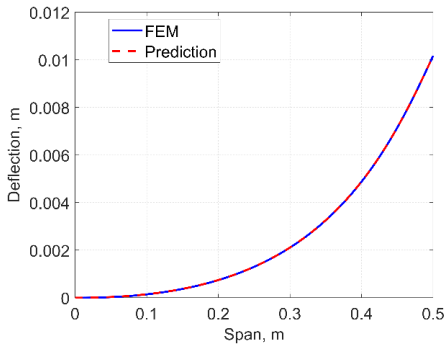

(b) deflection along the front array

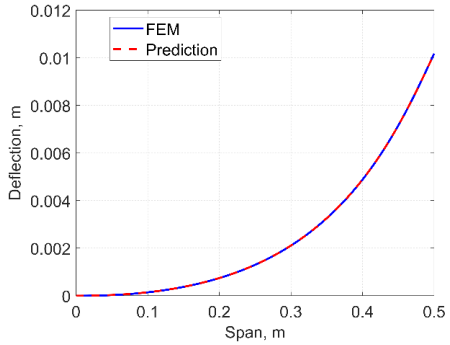

(c) deflection along the rear array

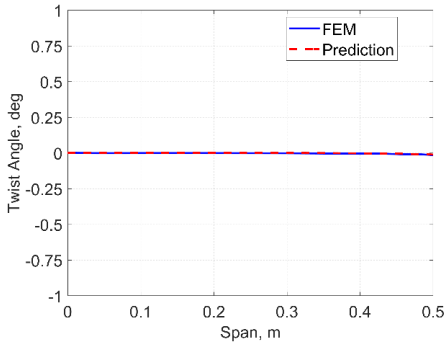

(d) twist along the neutral axis

Figure 6: Comparisons of deflections and twists along the neutral axis and strain measurement arrays on the simply tapered wing predicted by Ko's theory.

3.3 Simply swept wing

The simply swept solid wing studied is shown in Fig. 2c. Figure 7 shows the strains along the front and rear strain measurement arrays on the simply swept wing, obtained from the finite element simulation. Both strains on the two arrays almost linearly decreased to the tip. However, the strain on the rear array sharply increased around the root although the strain on the front array was similar to that for the unswept straight wing. The tendency of these strain distributions on the solid wing agreed with the case of the strain-sensing lines on the wing box, reported in Ref. [8]. Figure 8

shows the predicted deflections and twist along the two arrays obtained by Ko's theory. Ko's theory could accurately capture the deformations of the solid swept wing.

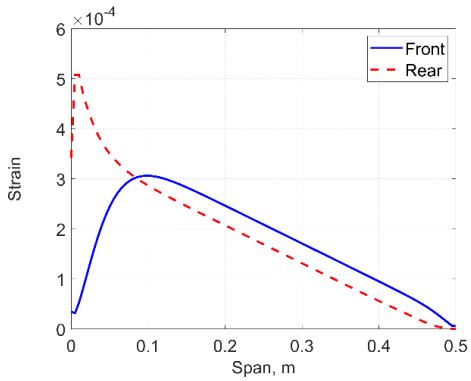

Figure 7: Strains along the front and rear arrays on the simply swept wing.

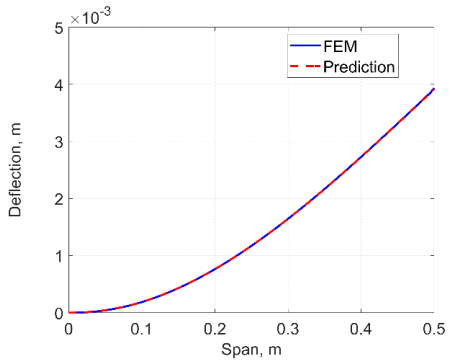

(a) deflection along the neutral axis

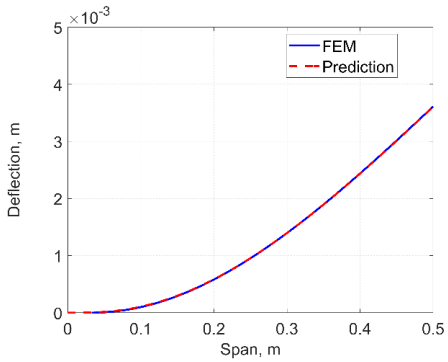

(b) deflection along the front array

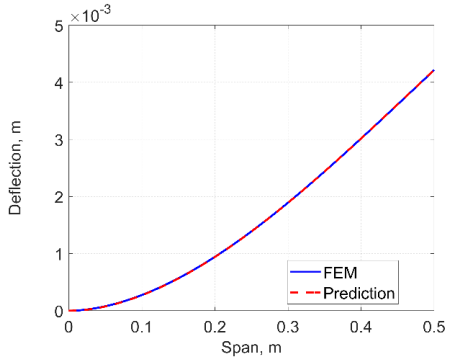

(c) deflection along the rear array

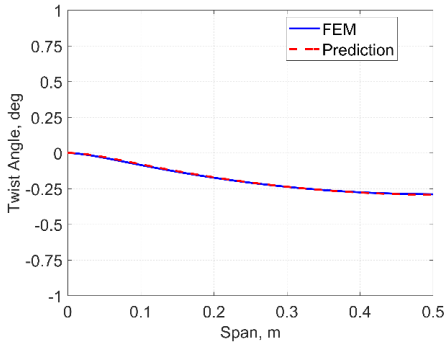

(d) twist along the neutral axis

Figure 8: Comparisons of deflections and twists along the neutral axis and strain measurement arrays on the simply swept wing predicted by Ko's theory.

3.4 Swept and tapered wing

The swept and tapered solid wing studied is shown in Fig. 2d. Figure 9 shows the strains along the front and rear strain measurement arrays on the swept and tapered wing, obtained from the finite element simulation. Both strains on the two arrays exhibited similar distributions except for the root region. The strain distributions on the two arrays were combinations of strain distributions

observed in the simply swept wing and the tapered wing. Figure 10 shows the predicted deflections and twist along the two arrays obtained by Ko's theory. According to the results, it was shown that Ko's theory could provide good predictions even for the deformations of the solid swept and tapered wing with the unsymmetric airfoil.

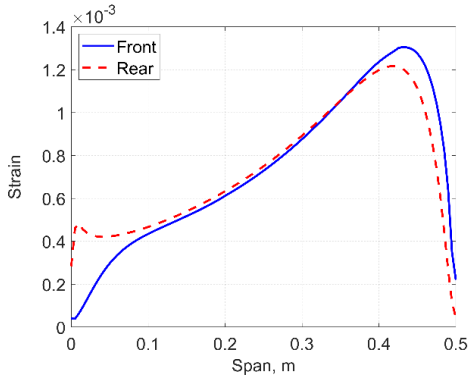

Figure 9: Strains along the front and rear arrays on the swept and tapered wing.

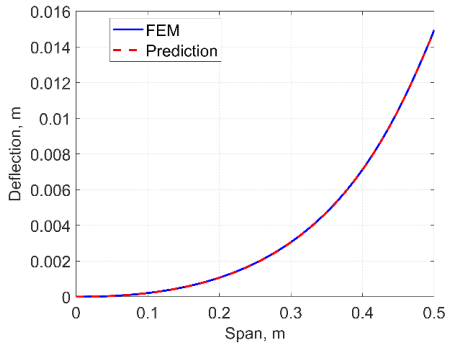

(a) deflection along the neutral axis

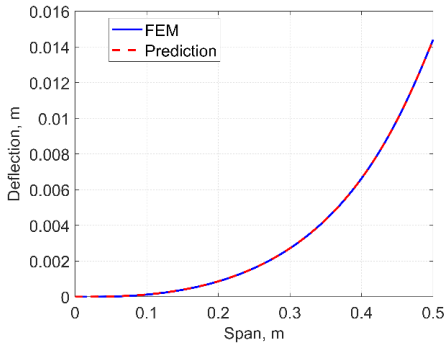

(b) deflection along the front array

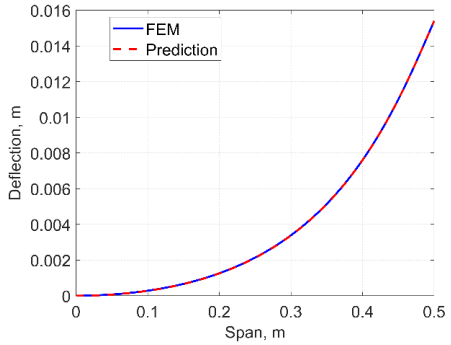

(c) deflection along the rear array

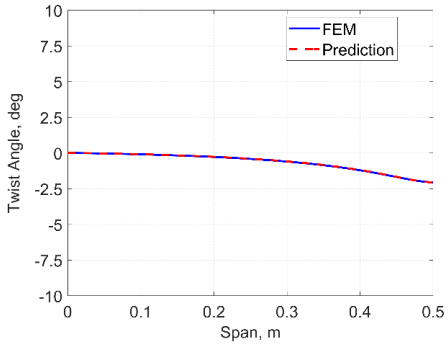

(d) twist along the neutral axis

Figure 10: Comparisons of deflections and twists along the neutral axis and strain measurement arrays on the swept and tapered wing predicted by Ko's theory.

In the preceding deformation predictions, all strains along the strain measurement arrays obtained from the simulations were used. However, there is a possibility to measure only a limited number

of strain sensing stations, *n*, along the strain measurement arrays in applications in wing models. Due to the nature of the integration procedure in Ko's theory, the sparse strain information along the arrays may impact the accuracy of the deformation prediction. The strain information could be compensated by interpolating strains on a limited number of strain sensing stations. Figure 11 shows the linearly interpolated strains along the front and rear arrays based on the different numbers of *n*. The strain distributions were sufficiently captured with $n \geq 10$. However, the interpolated strains with $n < 10$ exhibited significant differences from those with $n = 100$. Figure 12 shows the errors of the predicted deflections and twists to the finite element solutions at the tip of the wing. As the number of *n* decreased, the accuracy of the predictions for the deformations also reduced. The predicted deflections based on the interpolated strains with $n < 10$ exhibited errors of more than 5%. The errors in the predicted twists with $n = 4$ and 5 were lower than those with $n = 25$. However, those were due to the low resolutions and accuracies in strain and deflection distributions.

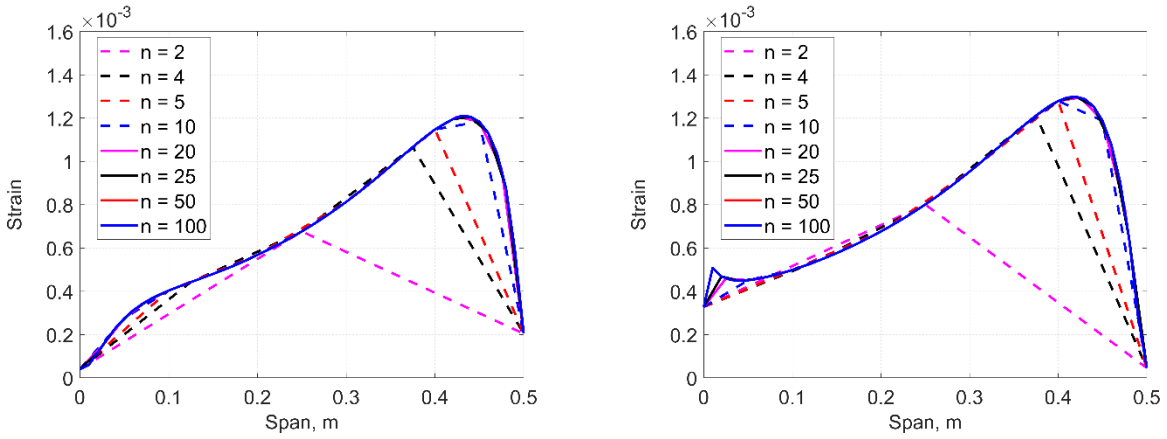

(a) strains along the front array (b) strains along the rear array

Figure 11: The strain distributions based on different numbers of strain sensing stations.

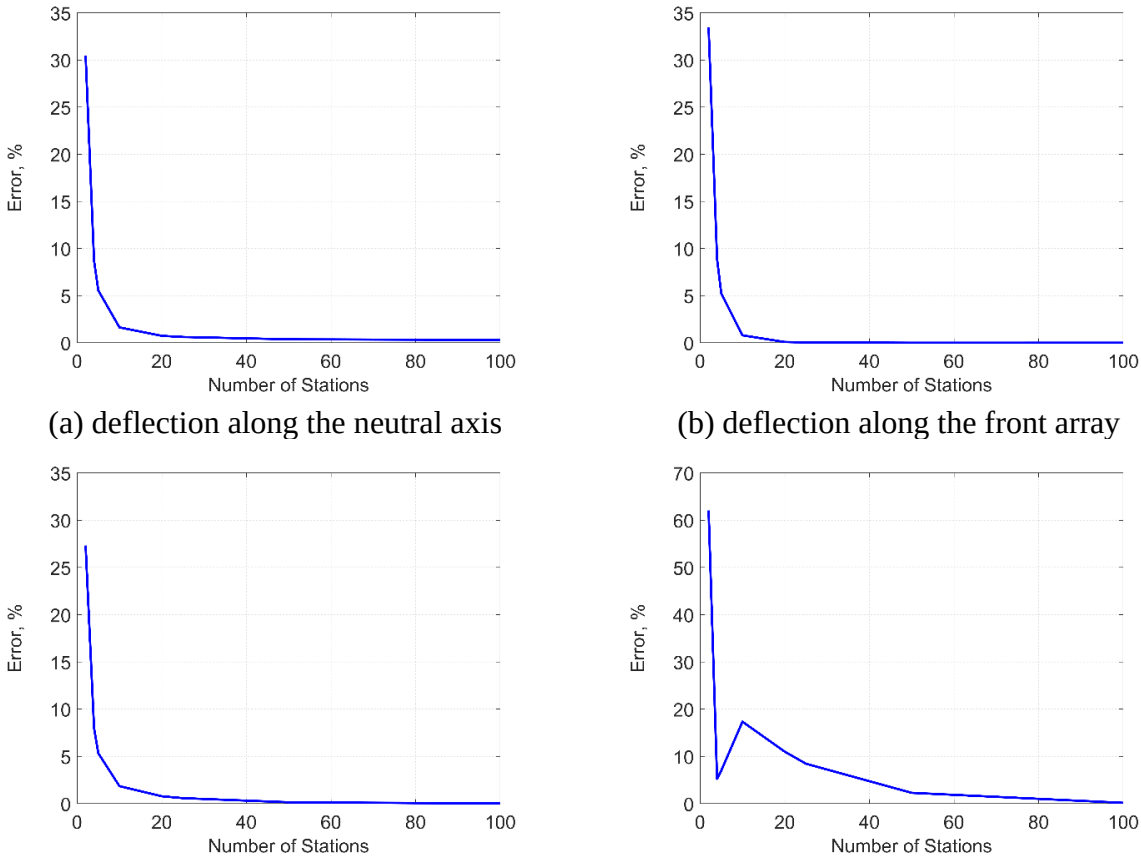

(a) deflection along the neutral axis

(b) deflection along the front array

(c) deflection along the rear array

(d) twist along the neutral axis

Figure 12: Errors of the predicted deflections and twists to the finite element solutions at the tip.

4 WING MODEL FOR TRANSONIC WIND TUNNEL TESTING

A wing model for transonic wind tunnel testing, which was supposed to be fabricated by AM technique based on fused deposition modeling (FDM), was designed to investigate the prediction accuracy for deformations of the wing model. The design of the wing model is described in this section. The numerical evaluations of aeroelastic deformations for the wing model were also performed based on Ko's theory.

4.1 Design of wing model

The swept and tapered solid wing in Fig. 2d was chosen as the model for the investigation. Figure 13 shows the wing model with a support beam for an installation into the wind tunnel. Two strain arrays were modeled as rectangular grooves with a width of 5 mm and a depth of 2.0 mm. Based on the preceding study, nine strain gages were installed along each strain measurement array starting at a 50mm-location from the root of the wing. The distance between each strain gauge was 50 mm. The rectangular grooves were closed with thin plates to form the aerodynamics. The

support beam made of nickel alloy, IN718, was inserted into the wing model, as shown in Fig. 13a. Young's modulus, Poisson's ratio, and density of the support beam structure were 170.0 GPa, 0.294, 8150.0 kg/m^3. Figure 14 shows the geometry of the support beam. The support beam had a square pocket to extract cables for strain gages out of the wing model. The wing structures were supposed to be fabricated by a 3D printer with polylactic acid (PLA) filaments. Young's modulus, Poisson's ratio, and density of the structures fabricated with the printing parameters were 2.551 GPa, 0.35, 1200.0 kg/m^3. Note that the wing model was assumed to be an isotropic structure based on the spanwise direction as spanwise bending and torsional characteristics would have critical influences on aeroelastic responses. Such an isotropic assumption was validated to provide sufficient accuracy in a prediction for the aeroelastic characteristics of additively manufactured wing models although it is known that additively manufactured structures exhibit anisotropic properties [4-6].

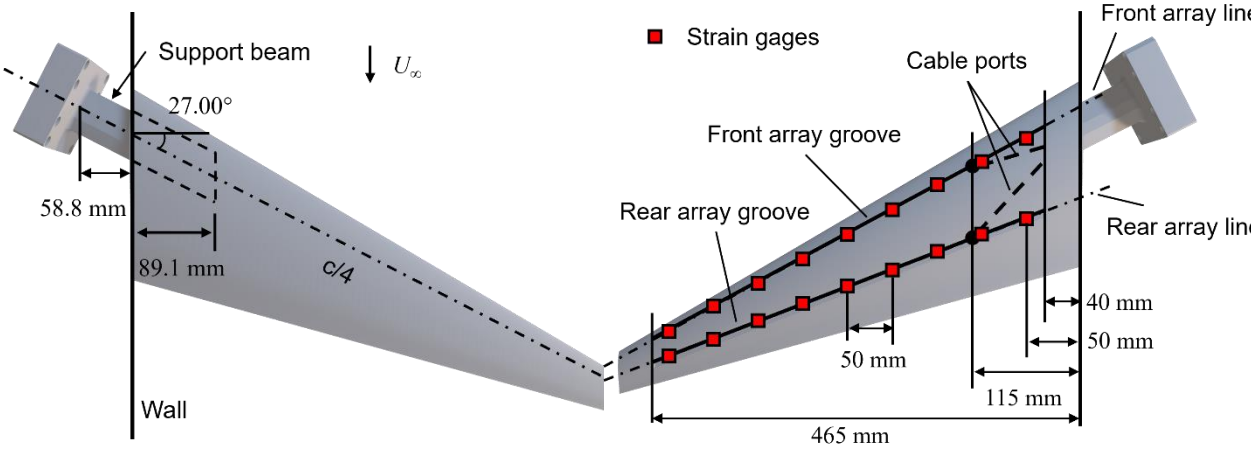

(a) top (b) bottom

Figure 13: The wing model for the transonic wind tunnel testing.

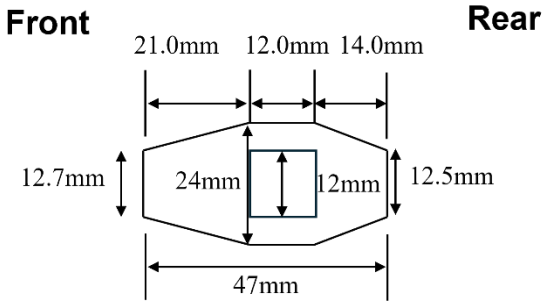

Figure 14: The cross-sectional geometry of the support beam.

4.2 Shape identification of wing model

The finite element model of the wing structure with the support beam was constructed to evaluate the structural and aeroelastic characteristics of the wing model. Figure 15 shows the finite element

model. The wing structure made of PLA and the support beam made of IN718 were modeled with 58,720 and 5,600 solid HEX8 elements, respectively. All nodes on the root of the support beam were fixed. Table 2 lists the lower natural frequencies of the wing model with the support beam. Figure 16 shows the lower out-of-plane (OOP) bending and torsional mode shapes. The first OOP bending mode was the lowest mode with a natural frequency of 52.44 Hz, which was followed by the second OOP bending mode. The first torsional mode was the fifth mode with a frequency of 441.18 Hz.

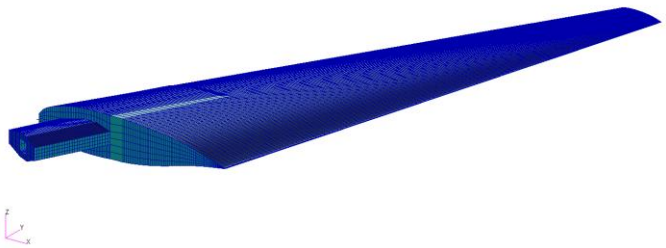

Figure 15: The finite element model of the wing with the support beam.

Table 2: Lower natural frequencies of the wing model.

Mode ID	Mode	Simulation, Hz
1	1st out-of-plane bending	52.44
2	2nd out-of-plane bending	149.74
3	1st in-plane bending	159.09
4	3rd out-of-plane bending	287.16
5	1st torsion	441.18
6	2nd in-plane bending	449.30

(a) mode 1: 1st out-of-plane bending

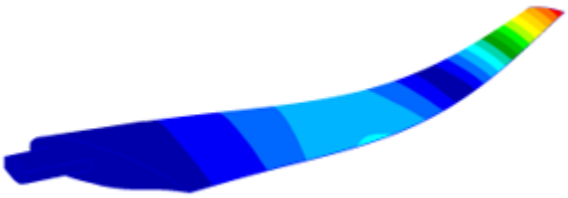

(b) mode 2: 2nd out-of-plane bending

(c) mode 4: 3rd out-of-plane bending

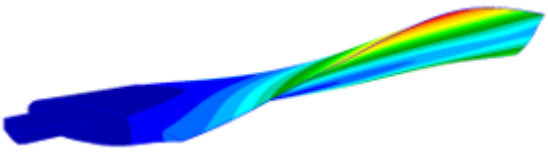

(d) mode 5: 1st torsion

Figure 16: The lower out-of-plane and torsional mode shapes.

A linear static aeroelastic analysis was then performed with the wing model. Aerodynamic panels were constructed with 1,000 panels (50 and 20 panels along the spanwise and chordwise directions). The aerodynamic loads were applied onto the upper surface of the wing. Figure 17 shows the static aeroelastic response of the wing model at Mach M = 0.9, dynamic pressure q = 29.217 kPa, and angle of attack α = 5°. The solutions were also compared with the predictions of Ko's theory based on the strain distributions along the strain measurement arrays, as shown in Fig. 18. The legends with "SG" indicate the interpolated strain distributions based on nine strain gages. The strains at the root and tip of the wing model were assumed to be zero due to the free boundary condition. The errors of the prediction to the finite element solutions for the deflections were less than 1%. Although the twist prediction at the tip showed a slight difference from the finite element solution, the average error of the twist between the prediction and the finite element solution was less than 5%. Therefore, the prediction could provide sufficient accuracy for deformation monitoring.

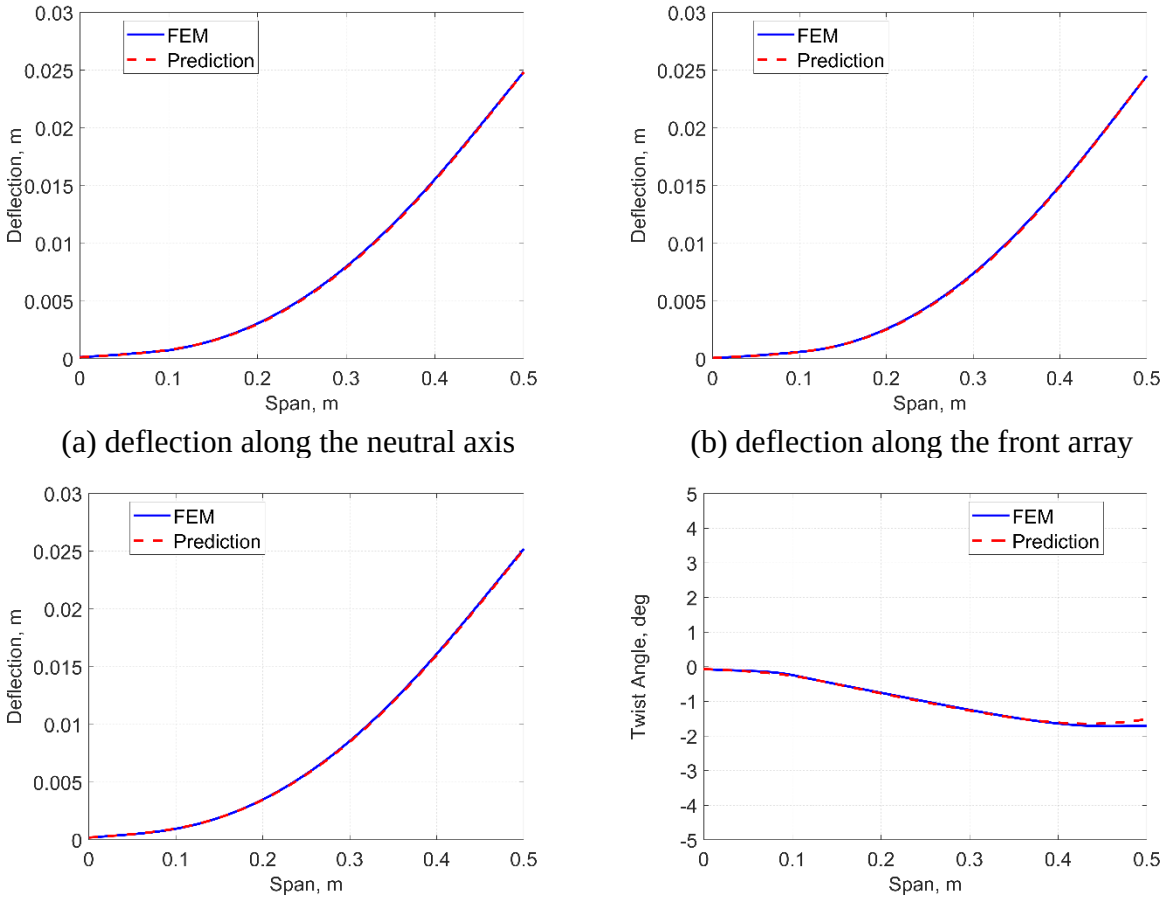

(a) deflection along the neutral axis

(b) deflection along the front array

(c) deflection along the rear array

(d) twist along the neutral axis

Figure 17: Static aeroelastic response of the wing model.

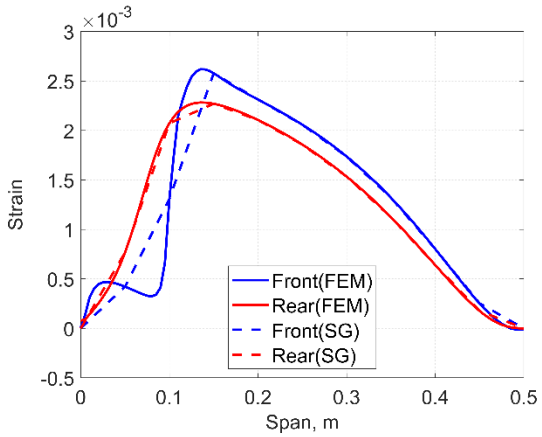

Figure 18: Strains along the front and rear arrays on the wing model.

5 CONCLUSIONS

This paper aimed to explore a structural shape identification technique for additively manufactured wing structures to enhance the capability of additively manufactured wing models for transonic wind tunnel testing. The objectives of this paper were 1) to explore the feasibility and capability of a method for the structural shape identification of additively manufactured solid wing structures based on strain measurements, and 2) to design an integrated structural monitoring system into AM-based transonic wing models, which enables the effective construction and investigation of aeroelastic wing models, and 3) to investigate the prediction accuracy for deformations of such a wing model. Ko's displacement theory was applied to identify structural deformations of wing structures based on strain measurements in this study.

Since the theory is mainly studied for simple symmetric beams or wings, the feasibility of the theory to identify structural deformations of unsymmetric solid wings with a supercritical airfoil was investigated. Based on the numerical results, it was shown that Ko's theory could provide good predictions even for the deformations of the solid swept and tapered wing with the unsymmetric airfoil.

As a course toward the effective structural monitoring system, a wing model with strain measurement arrays, which was compatible with the AM technique, was designed. The aeroelastic simulation proved that the shape prediction of such a wing model based on the designed strain measurement system and Ko's theory could provide sufficient accuracy for deformation monitoring.

In future work, the designed wing model will be constructed to validate the results of the numerical studies. The aeroelastic characteristics of the fabricated wing model will be evaluated by performing a transonic wind tunnel experiment. The wind tunnel test will be conducted in the Transonic Wind Tunnel Göttingen (DNW-TWG) at the German Aerospace Center (DLR).

REFERENCES

[1] Tsushima, N., Higuchi, R., and Yamamoto, K. Correlation studies of different decoupled two-scale simulations for lattice structures. *Aerospace,* 2023, 10(8), 723.

[2] Tsushima, N., and Higuchi, R. Stiffness and strength evaluation of lattice-based mechanical metamaterials by decoupled two-scale analysis. *Materials Today Communications,* 2022, 31, 103598.

[3] Moioli, M., Reinbold, C., Sørensen, K., and Breitsamter, C. Investigation of additively manufactured wind tunnel models with integrated pressure taps for vortex flow analysis. *Aerospace,* 2019, 6(10), 113.

[4] Tsushima, N., Saitoh, K., and Nakakita, K. Structural and aeroelastic characteristics of wing model for transonic flutter wind tunnel test fabricated by additive manufacturing with AlSi10Mg alloys. *Aerospace Science and Technology,* 2023, 140, 108476.

[5] Tsushima, N., Saitoh, K., Arizono, H., and Nakakita, K. Structural and aeroelastic studies of wing model with metal additive manufacturing for transonic wind tunnel test by NACA 0008 example. *Aerospace,* 2021, 8(8), 200.

[6] Tsushima, N., Tamayama, M., Arizono, H., and Makihara, K. Geometrically nonlinear aeroelastic characteristics of highly flexible wing fabricated by additive manufacturing. *Aerospace Science and Technology,* 2021, 117, 106923.

[7] Gherlone, M., Cerracchio, P., and Mattone, M. Shape sensing methods: Review and experimental comparison on a wing-shaped plate. *Progress in Aerospace Sciences,* 2018, 99, 14-26.

[8] Ko, W. L., and Fleischer, V. T. Further development of Ko displacement theory for deformed shape predictions of nonuniform aerospace structures. NASA/TP-2009-214643, NASA.

[9] Bogert, P., Haugse, E., and Gehrki, R. Structural shape identification from experimental strains using a modal transformation technique. *44th AIAA/ASME/ASCE/AHS/ASC Structures, Structural Dynamics, and Materials Conference*. 2003, AIAA-2003-1626.

[10] Fang, L., Chen, T., Li, R., and Liu, S. Application of embedded fiber bragg grating (FBG) sensors in monitoring health to 3D printing structures. *IEEE Sensors Journal,* 2016, 16(17), 6604-6610.

[11] Yan, W., Ma, S., Wang, H., and Zhang, X. Fiber bragg grating online packaging technology based on 3D printing. *Optics & Laser Technology,* 2020, 131, 106443.

[12] Palma, P. D., Iadicicco, A., and Campopiano, S. Study of fiber bragg gratings embedded in 3D-printed patches for deformation monitoring. *IEEE Sensors Journal,* 2020, 20(22), 13379-13386.

[13] Nomura, T. Conceptual design of future passenger aircraft aimed at reducing fuel consumption, Dec. 2013. JAXA-RR-13-007, Japan Aerospace Exploration Agency, 1-14.

COPYRIGHT STATEMENT